



RESEARCH LETTER

10.1002/2015GL064585

Key Points:

- A new method for obtaining SAR image offsets between different satellite sensors
- Improved near-field coseismic displacements of the Bhuj earthquake
- The Bhuj earthquake had a compact source at depth with short rise time

Supporting Information:

- Figure S1
- Figure S2
- Figure S3
- Figure S4
- Figure S5
- Figure S6
- Figure S7
- Text S1 and Captions of Figures S1–S7
- Text S2
- Text S3
- Text S4
- Text S5

Correspondence to:

T. Wang,
wang.teng@gmail.com

Citation:

Wang, T., S. Wei, and S. Jónsson (2015), Coseismic displacements from SAR image offsets between different satellite sensors: Application to the 2001 Bhuj (India) earthquake, *Geophys. Res. Lett.*, **42**, doi:10.1002/2015GL064585.

Received 15 MAY 2015

Accepted 11 AUG 2015

Accepted article online 14 AUG 2015

Coseismic displacements from SAR image offsets between different satellite sensors: Application to the 2001 Bhuj (India) earthquake

Teng Wang^{1,2}, Shengji Wei³, and Sigurjón Jónsson¹

¹Division of Physical Sciences and Engineering, King Abdullah University of Science and Technology, Thuwal, Saudi Arabia,

²Now at Huffington Department of Earth Sciences, Southern Methodist University, Dallas, Texas, USA, ³Earth Observatory of Singapore, Nanyang Technological University, Singapore

Abstract Synthetic aperture radar (SAR) image offset tracking is increasingly being used for measuring ground displacements, e.g., due to earthquakes and landslide movement. However, this technique has been applied only to images acquired by the same or identical satellites. Here we propose a novel approach for determining offsets between images acquired by different satellite sensors, extending the usability of existing SAR image archives. The offsets are measured between two multiimage reflectivity maps obtained from different SAR data sets, which provide significantly better results than with single preevent and postevent images. Application to the 2001 M_w 7.6 Bhuj earthquake reveals, for the first time, its near-field deformation using multiple preearthquake ERS and postearthquake Envisat images. The rupture model estimated from these cross-sensor offsets and teleseismic waveforms shows a compact fault slip pattern with fairly short rise times (<3 s) and a large stress drop (20 MPa), explaining the intense shaking observed in the earthquake.

1. Introduction

Synthetic aperture radar (SAR) imaging is widely used for mapping ground movements with two main approaches: one is through computing coherent phase differences, i.e., interferometric SAR (InSAR) [e.g., *Massonnet et al.*, 1993], and the other is through estimating pixel offsets (offset tracking) between preevent and postevent images [e.g., *Michel et al.*, 1999]. The most striking limitation of InSAR is the decorrelation between SAR images, which can be caused by high displacement gradients, large spatial baselines, dense vegetation, different acquisition modes, and different carrier wave frequencies [Zebker and Villasenor, 1992]. InSAR is sensitive to all these decorrelation factors and thus often fails in obtaining near-field measurements in earthquake studies [e.g., *Schmidt and Bürgmann*, 2006]. Offset tracking, on the other hand, is relatively insensitive to InSAR decorrelation and has been used successfully in many cases where InSAR has failed [e.g., *Pathier et al.*, 2006; *Elliott et al.*, 2007; *Wang and Jónsson*, 2015]. However, SAR pixel offsets have always, up to now, been calculated using images acquired by the same SAR satellite or identical satellites, which limits measurements of some earthquakes. For example, following the failure of the gyroscopes aboard the European ERS-2 satellite in January 2001, there was a “data gap” period before the Envisat satellite became fully operational in September 2002 [European Space Agency, 2001]. Coherent ERS image pairs are usually missing for mapping the coseismic deformation of earthquakes that occurred during this period. In these cases, neither InSAR (including multiaperture interferometry [Bechor and Zebker, 2006]) nor standard offset tracking can provide reliable coseismic displacement measurements.

The devastating M_w 7.6 Bhuj (India) earthquake, which occurred on 26 January 2001 and killed ~20,000 people [Hough et al., 2002], is one such event that took place during the data gap period. Almost no information exists about the near-field coseismic displacement field of this earthquake because of a lack of coherent ERS image pairs. Scientists working on the Bhuj event therefore struggled to constrain the parameters of the fault rupture models of the earthquake. Existing geodetic observations include sparsely distributed leveling and gravity data [Chandrasekhar et al., 2004; Wallace et al., 2006], flooding pattern variations observed in optical satellite images [Gahalaut and Bürgmann, 2004], isolated ERS interferogram patches [Schmidt and Bürgmann, 2006], and image offsets from optical images [Copley et al., 2011]. These geodetic observations, however, failed to provide information about the near-field deformation of the earthquake. Consequently, rupture models derived

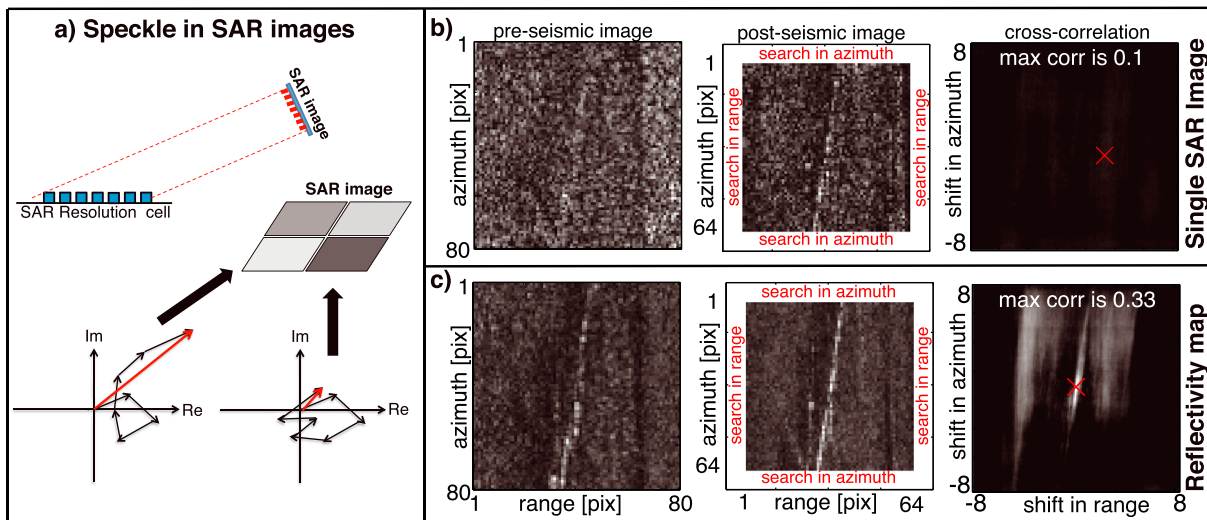


Figure 1. Speckle in SAR images and its effect on cross-correlation calculations between images. (a) Schematic plot of how phase information results in random speckle patterns in the amplitude of a SAR image. Re and Im represent the real and imaginary parts of the complex SAR signal. (b) Typical (right) cross-sensor correlation between (left) pre-seismic and (middle) post-seismic subimages for a single SAR image cross correlation. The red cross shows the location of the cross-correlation peak. (c) Same as Figure 1b except for cross correlation of multiimage reflectivity maps. Note the increase of the peak cross correlation from 0.1 to 0.33.

from teleseismic only [Antolik and Dreger, 2003], geodetic only [Schmidt and Bürgmann, 2006], and joint inversions [Copley et al., 2011] show very different near-field deformation characteristics. In particular, both the depth and the amplitude of the peak slip vary significantly in these models. The disparity in the source models makes it difficult to resolve an unanswered and important question about this earthquake: What earthquake fault source properties of this $M_w 7.6$ event could generate the intense shaking that was felt on the entire Indian subcontinent [Hough et al., 2002]? Reliable near-field displacement measurements are essential to answer this question and to provide more insight into this devastating earthquake.

With existing ERS images from before and Envisat images from after the Bhuj earthquake, we explored approaches to retrieving coseismic deformation from these two sets of data. ERS-Envisat interferometry is possible, but only when the temporal baseline is short and the spatial baseline is close to 2 km to compensate for the 31 MHz carrier frequency difference. This orbital configuration was engineered during the “ERS-Envisat consolation period” between 27 September 2007 and 12 February 2008 [Santoro et al., 2007] with the data primarily used for digital elevation model (DEM) generation [e.g., Wegmüller et al., 2009]. ERS-Envisat interferometry is thus not applicable to the Bhuj case; rather, we have to consider how to calculate pixel offsets between the ERS and Envisat images. Even though pixel offsets between different optical sensors (cross sensors) have been widely applied to map earthquake-induced deformation [e.g., Ayoub et al., 2009] and to study dike intrusions [e.g., Hollingsworth et al., 2012], there are few, if any, studies on using SAR images from different satellites to derive coseismic displacements. A cross-sensor SAR offset technique for cases like the Bhuj earthquake is therefore needed.

SAR image offsets are estimated from similarities between subimages (i.e., cross-correlation windows) distributed throughout the imaged area [Michel et al., 1999]. The similarity comes from the coherent speckle patterns and the ground reflectivity. When two SAR images are completely incoherent, such as in images from two different sensors, the speckle patterns are not correlated (Figure 1). The reflectivity of targets with similar scattering characteristics, on the other hand, can still provide useful features for estimating offsets. With large numbers of archived SAR images covering the same region, it is possible to suppress decorrelated speckle noise and to enhance the correlated reflectivity. Here we exploit this possibility and present a novel approach that allows offsets between SAR images acquired by different satellites to be calculated. Application to the 2001 Bhuj earthquake reveals, for the first time, its near-field coseismic displacement field immediately above the hypocenter from cross-sensor ERS and Envisat images. We then present our estimation results by jointly using the new SAR image offsets together with teleseismic waveforms to constrain the rupture model of this rare intraplate event.

2. Method

2.1. Reflectivity Maps From Multiple Preseismic and Postseismic SAR Images

The principle of image offset estimation is to maximize the similarity between two subimages by shifting one with respect to the other. This procedure can be implemented by calculating the normalized cross correlation using the amplitude information of the two subimages [e.g., *Michel et al.*, 1999]. The peak location in the obtained cross-correlation surface indicates the offsets between these two subimages in two dimensions (e.g., Figures 1b and 1c). The accuracy and reliability of the estimated offset is a function of the cross-correlation peak, which relies on the signal-to-clutter ratio of the two subimages [*Bamler and Eineder*, 2005]. Here the signal refers to correlated image features representing the illuminated ground. This basic idea is widely applied to both optical and radar data. For optical images, image features are representations of the surface reflectivity of the sunlight [e.g., *Leprince et al.*, 2007], while for SAR sensors, image features are attributed in part to the surface reflectivity of the radar signal and in part to speckle patterns [*De Zan*, 2014].

Each recorded complex value in a focused SAR image is the coherent sum of the radar echoes reflected back from the wavelength size scatterers within a resolution cell. The amplitude mainly depends on the geometry, roughness, and material properties of the ground scatterers [*Bamler and Hartl*, 1998]. The phase depends on the sensor-target distance and the scatterer arrangement, and it can lead to a random (Rayleigh distributed) amplitude component, which is known as the speckle pattern in SAR amplitude maps (Figure 1a). SAR images from the same sensor have spatially correlated (statistically homogeneous) speckle patterns, given that scatterers maintain stable distribution and reflectivity [*De Zan*, 2014]. However, phase-related speckle is highly sensitive to many decorrelation aspects, e.g., changes in the ground surface (the temporal decorrelation), variations in the imaging geometry (the geometrical decorrelation), and/or differences in the carrier wave frequency between cross-sensor SAR images [e.g., *Zebker and Villasenor*, 1992; *Perissin et al.*, 2006]. The reflectivity recorded in SAR amplitude maps, on the other hand, is much more resistant to these decorrelation aspects.

To achieve cross-sensor SAR image offsets, the reflectivity, instead of the speckle, is the main source of similarity between cross-correlation windows, and we thus need to suppress the speckle noise before cross-correlating subimages. Many speckle filterers, in particular spatial filterers, have been proposed since the early days of SAR studies [e.g., *Lee*, 1986], but spatial filtering comes at the expense of spatial resolution. After years of systematic SAR image acquisition, we can now take advantage of the temporal averaging instead of spatial smoothing to suppress the speckle noise and generate what has been called a multiimage SAR reflectivity map [*Ferretti et al.*, 2001]. We then apply our previously developed coregistration method [*Wang et al.*, 2014], which considers topographic effects and timing errors, to resample the preseismic and postseismic images onto the grid of the images acquired close in time to the earthquake. We generate the multiimage reflectivity maps by averaging the SAR amplitude maps, which strongly reduces the speckle noise, yet preserves the spatial resolution (Figure 1c). We assume that the preseismic and postseismic displacements are much smaller than the coseismic displacements, which has been reported to be the case for the Bhuj earthquake [*Chandrasekhar et al.*, 2009].

2.2. Coregistration of SAR Reflective Maps From Different Sensors

Offsets between preseismic and postseismic images are attributed to the coseismic displacement as well as to differences in the imaging geometry. Because SAR images from different satellites are generally acquired from very different orbital geometries, large orbital offset variations throughout the whole scene can result. This orbital offset variation is often larger than the size of a typical cross-correlation window (e.g., 64-by-64 pixels). The offset caused by coseismic displacement, on the other hand, is only a small fraction of the window size (i.e., typically less than 15 m or 2–3 pixels of ERS and Envisat data). We therefore need to resample one reflectivity map onto the grid of the other one before carrying out the cross-correlation calculation.

We can calculate the expected geometric offsets between images acquired from different sensors based on the satellite orbital information and a DEM. For each pixel of the postseismic reflectivity map, we calculate the corresponding position on the Earth. Using this position, we then calculate the pixel coordinates in the preseismic SAR image [*Sansosti et al.*, 2006; *Wang et al.*, 2014]. In this way, we generate a pixel-by-pixel geometric offset map and use this map to resample the preseismic reflectivity map onto the grid of the postseismic map (or vice versa). After the resampling, we estimate possible offsets caused by absolute geolocation errors using several large and sparsely distributed cross-correlation windows (e.g., 256-by-256 pixels) in undeformed

areas. We then correct only the constant shift between the two reflectivity maps before estimating the coseismic displacements to avoid losing any of the deformation signal during the coregistration procedure. The coregistration step presented here is also important for eliminating topography-related components in the derived coseismic displacement map.

2.3. Calculation of Cross-Sensor SAR Image Offsets

To estimate the coseismic displacements, we distribute cross-correlation windows throughout the two coregistered reflectivity maps. In urban areas, we can center the cross-correlation windows on some detected bright pixels with high reflectivity, such as that from point-like targets, to improve the offset measurements [Wang and Jónsson, 2015]. In rural areas, accurate offsets can often be obtained from macroscopic features in the reflective maps, such as from roads, edges of fields, and ridge corners [e.g., Elliott et al., 2007]. With such features, using a uniform distribution of cross-correlation windows is the easiest way to increase the measurement coverage. Depending on ground conditions, we need to choose one or to use both strategies to fulfill the balance between the accuracy and the spatial coverage of the measurement. Although we used our own software to process the data, the proposed method can be easily implemented in existing SAR/InSAR packages, as we use a cross-correlation calculation to estimate the offsets similar to that in the standard SAR offset tracking method, e.g., the process implemented in the ROI_pac software package [Rosen et al., 2004].

The improvement from using multiple images, instead of single SAR images, is clearly visible, both in the quality of the reflectivity map and in the derived cross-correlation (Figures 1b and 1c). Compared with offsets derived from coherent speckles, the accuracy of the cross-sensor result is lower as the reflectivity feature size is at the pixel-spacing level, which is much larger than the speckle pattern that is related to the wavelength size scatterers (about 1/100 of the pixel spacing for ERS and Envisat images). Nevertheless, decorrelation effects do not much affect the surface reflectivity, allowing us to obtain new geodetic measurements using archived cross-sensor SAR images.

3. Application to the 2001 M_w 7.6 Bhuj Earthquake

3.1. Coseismic Displacement Derived From ERS-Envisat Image Offsets

The M_w 7.6 Bhuj earthquake struck northwest India in the morning of 26 January 2001, causing nearly 20,000 casualties, 166,000 injuries and widespread destruction [Hough et al., 2002]. Previous studies suggest that the maximum surface displacement should have been a few meters in the epicenter area, although no direct measurements have been available [e.g., Chandrasekhar et al., 2004; Schmidt and Bürgmann, 2006]. Three ERS satellite tracks (descending tracks T234 and T463; ascending track T84) cover the epicentral area, but the failure of the gyroscope and seasonal flooding caused serious decorrelation in all coseismic ERS interferograms. Coherence was retained only on a few isolated patches in the far field, and reliable phase unwrapping became almost impossible [Schmidt and Bürgmann, 2006] (supporting information Figure S1). We also calculated the offsets between the preseismic and postseismic ERS images. However, the results are not useable, as the Doppler center differences between these images and the speckle noise seriously reduce the reliability of the cross-correlation operator. Moreover, only a few ERS-2 images were acquired after the event (1 from track 463, 1 from track 84, and 10 from Track 234, but only 2 are usable), and therefore, the multiimage averaging procedure could not be applied to reduce the speckle noise. During the lifetime of the Envisat satellite, several images were acquired covering the same area as the ERS descending images (Figures 2 and 3), but unfortunately, no ascending (track T84) Envisat acquisitions were carried out.

We separately coregistered the preearthquake ERS and postearthquake Envisat data sets to generate two multiimage reflectivity maps, and we then resampled the ERS map onto the grid of the Envisat map using orbital information and the Shuttle Radar Topography Mission DEM (see Figure S2 for acquisition times and baseline distributions). Considering that the earthquake occurred in a rural area, although with many sparsely distributed houses accommodating the dense population, we first uniformly distributed nonoverlapping 64-by-64 pixel cross-correlation windows (64-pixel step) throughout the reflectivity maps to estimate the coseismic displacement field. We then added a few thousand more windows on detected strong reflectors to improve the displacement map [Wang and Jónsson, 2015]. The overall improvement from using multiimage reflectivity maps, instead of single images, is evident from comparing the offsets directly (Figures 2a and 2b) and also from the significant increase in high cross-correlation measurements (Figure 2c).

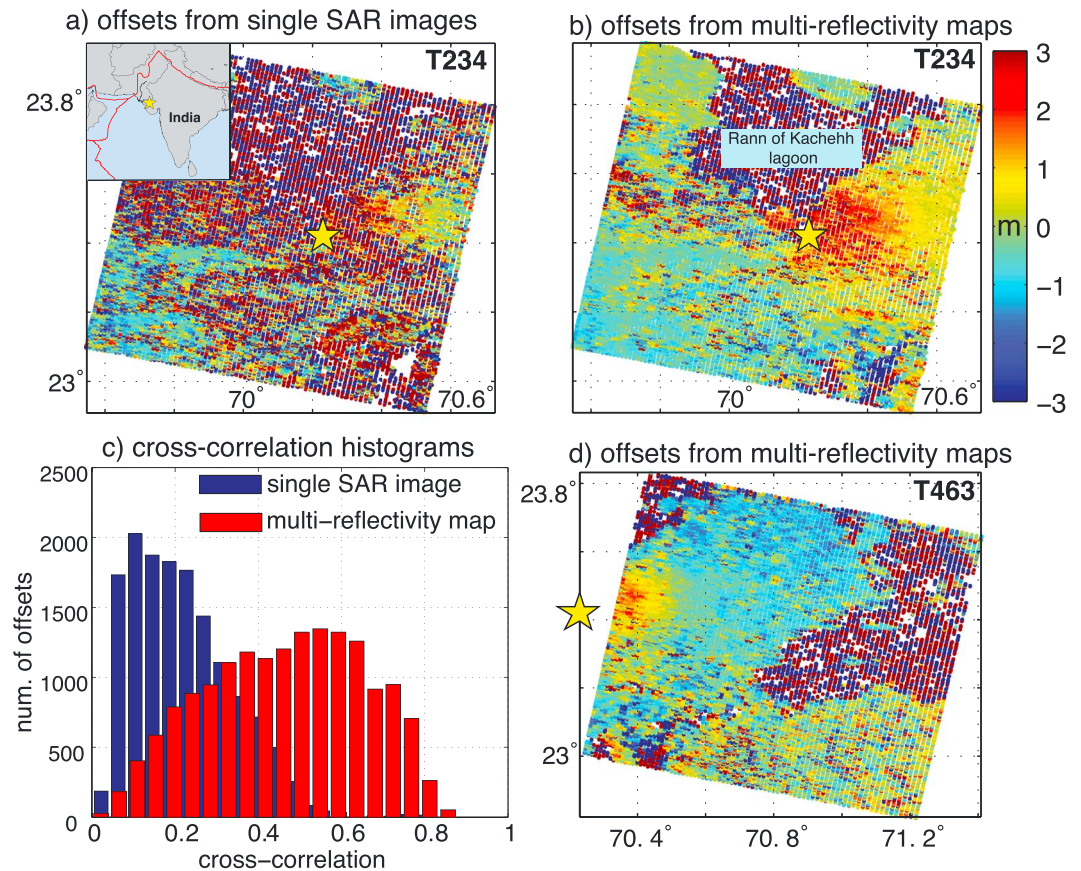


Figure 2. Cross-sensor ERS-Envisat range offsets showing the near-field deformation of the Bhuj earthquake, with red indicating ground movement toward the satellites, i.e., mainly uplift. Comparisons show that offsets from (a) single SAR images can be significantly improved by using (b) multiimage reflectivity maps, resulting in (c) higher cross-correlation values. (d) The result from another descending track (T463) is shown. The inset in Figure 2a shows the location (yellow star) of the Bhuj earthquake far from plate boundaries (red lines).

The ERS-Envisat offsets from the two parallel descending tracks clearly retrieve the near- and far-field coseismic deformation related to the 2001 Bhuj earthquake (Figures 2b and 2d). The results indicate that the hanging wall moved about 2 m up in the line-of-sight (LOS) direction toward the satellite. Although we cannot get any information from the area north of the epicenter, because of the Rann of Kachehh lagoon, the measurement coverage is still much better and more complete near the epicenter than the InSAR patches used in previous studies [e.g., Schmidt and Bürgmann, 2006; Copley et al., 2011].

We used a teleseismic-derived slip model to generate synthetic surface displacements in the radar's LOS direction, and then we used the predicted displacements to generate two quadtree subsampling masks [Jónsson et al., 2002], on which we downsampled the observed offsets from tracks T234 and T463, resulting in 259 and 539 data points, respectively (Figure 3). By calculating the standard deviation of offsets about 30 km away from the epicenter, we assessed the offset accuracy to be about 0.6 m, or 1/10 of the pixel spacing in the range direction of both tracks. In the azimuth direction, the observed pattern shows that the coseismic deformation in the satellite's flying direction (mainly the NS component) was small (less than 1 m) compared with that of the vertical displacement (Figure S7).

3.2. A Rupture Model Derived From SAR Offsets and Teleseismic Waveform Data

We used the downsampled ERS-Envisat offsets (both azimuth and range offsets) in conjunction with 58 *P* and 61 *SH* waves at teleseismic distance (30°–90°, Figure S3) to constrain the finite rupture process of the earthquake [Ji et al., 2002]. To demonstrate the resolution improvement from jointly using the two data sets, we conducted several checkerboard tests in which the joint estimation recovered the slip model much better

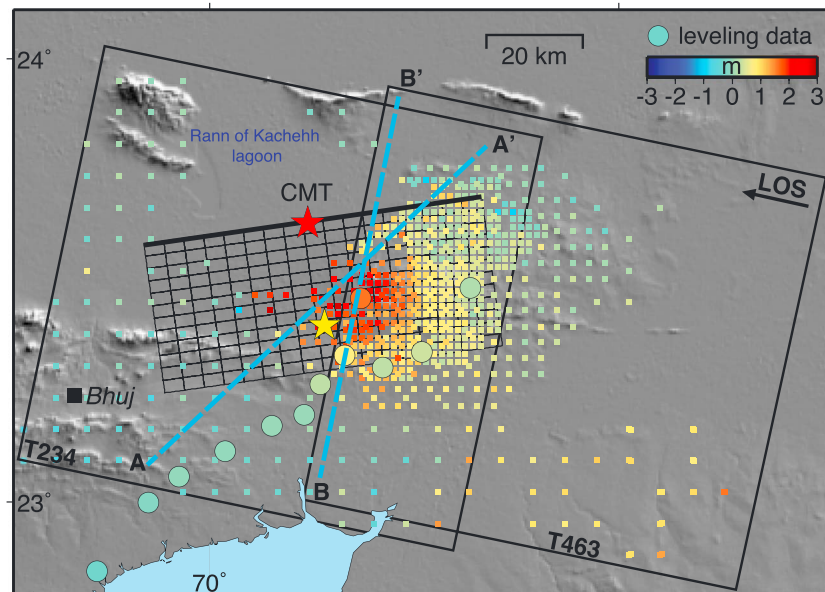


Figure 3. Downsampled displacement measurements from the two descending tracks T234 and T463 (from Figures 2b and 2d). Red indicates movement up and/or east toward the satellite's line-of-sight (LOS) direction (mainly uplift). The leveling height changes are shown with green circles. The centroid location determined in this study (yellow star) is located more than 30 km south of the global centroid moment tensor location (red star). The rectangle mesh shows the surface projection of the south dipping subfaults used in the finite-fault estimation (see Figure 4). Profiles A-A' and B-B' are shown in Figures 4d and 4e.

than did the teleseismic estimation by itself (Figure S4). We then applied the same optimization setup to the real data. The result is displayed in Figure 4, and the corresponding static and teleseismic waveform fits are shown in Figures S5–S7, in which both the seismic and geodetic fit well (optimization data are provided in the supporting information).

The rupture model indicates a compact slip distribution with a peak slip of ~ 9 m, mainly concentrated at depths ranging from 8 to 30 km, and most of the moment was released in the first 15 s (Figures 4a–4c). The rise time for most of the large slip patches was very short (< 3 s), corresponding to high slip rate (slip/rise time) of about 3.0 m/s. This high slip rate and the low attenuation in the crust of the Indian subcontinent are likely responsible for the widely felt ground shaking as reported by *Hough et al.* [2002]. Our results indicate a high static stress drop (~ 20 MPa) and a very short rise time. The radiated earthquake energy was thus high and concentrated in time, consistent with observations by *Singh et al.* [2004]. The high stress drop is also consistent with the findings by other groups [e.g., *Negishi et al.*, 2002 and *Copley et al.*, 2011].

4. Discussion and Conclusions

The Bhuj earthquake was located several hundred kilometers away from the nearest plate boundary, providing a unique opportunity to study a large earthquake in the interior of a continent (Figure 2, inset). However, the lack of near-field data resulted in poor constraints of source model parameters, particularly of the upward termination of the fault rupture. The ERS-Envisat SAR offsets presented here significantly improve the fault slip resolution of the shallow parts of the fault plane. The resulting compact source indicates that only a fraction of the seismogenic crust was ruptured in the earthquake, suggesting that more earthquakes can be expected in the future.

To assess further the importance of near-field geodetic measurements in earthquake source modeling, we calculated the predicted surface displacements (in the radar's LOS directions) using source models from previous studies on the Bhuj earthquake. A comparison of the two LOS-displacement profiles across the epicenter areas (Figures 4d and 4e) indicates that the far-field displacements are underestimated by the teleseismic-only model from *Antolik and Dreger* [2003] and the near-field displacements overestimated by

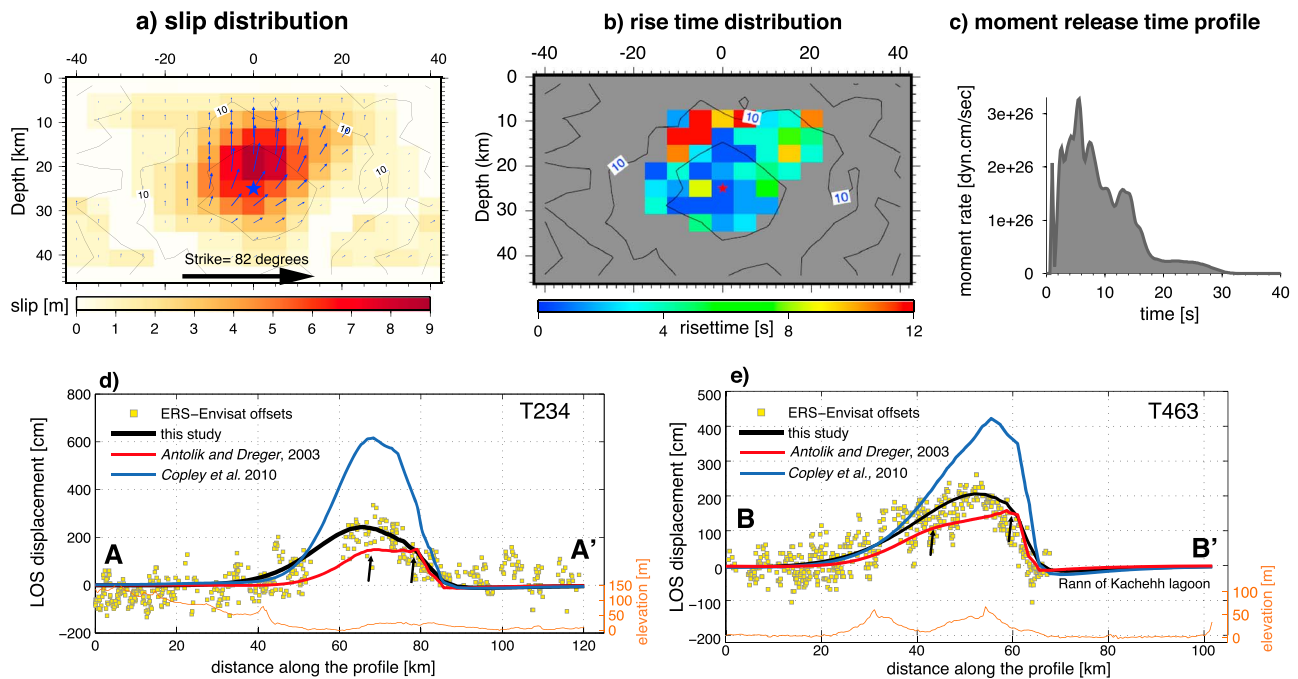


Figure 4. Estimated source model of the Bhuj earthquake from using both teleseismic and offset data (both azimuth and range offsets). (a) Fault slip magnitude and rake; (b) rise time with the hypocenter marked as a red star and contours indicating rupture times; (c) the moment-rate function of the rupture model. (d and e) Line-of-sight surface displacement observations (yellow squares) along profiles A-A' and B-B' (shown in Figure 3) in comparison to displacement predictions of the estimated source model (black line), two other source models, and topography (orange line). Small black arrows point to two deformation peaks predicted by *Antolik and Dreger* [2003] model.

a factor of 2 by the model from *Copley et al.* [2011]. The major difference between our slip model and the one by *Antolik and Dreger* [2003] is the relative lack of slip at intermediate depths (10–15 km) in their model. The shallow and deep slip asperities in their model predict two peaks in the profiles, as indicated by the arrows in Figure 4d. This feature is not observed in our geodetic data. *Antolik and Dreger* [2003] argued that the shallow asperity was required to explain the intensity pattern near the source [*Hough et al.*, 2002]. However, the shaking intensity was probably also strongly dependent on the local velocity structure (i.e., a basin), particularly the shallow geotechnical layers near the surface, which was not considered in *Antolik and Dreger* [2003]. The model proposed by *Copley et al.* [2011] also has significant slip at shallow depths but of much larger amplitude than that of *Antolik and Dreger* [2003], which produces larger ground deformation than observed in our data. The overestimated shallow slip, as well as the peak slip, is probably due to unwrapping errors in the InSAR data they used and to the lack of near-field information. Overall, their model leads to an overestimation of the static stress drop. The displacement profiles clearly demonstrate that without near-field geodetic observations, it can be difficult to derive reliable rupture models. Furthermore, the addition of the near-field geodetic data in the estimation leads to a compact source and thus better constraints of the rise time of the earthquake, which was fairly short (<3 s) and had not been reported previously for this earthquake.

With the application to the Bhuj earthquake, we have shown that our cross-sensor method overcomes the restrictions of using only same-sensor SAR images to extract coseismic deformation. Although the accuracy of the reflectivity-derived offsets in our method is lower than InSAR and same-sensor speckle-derived offsets, our method provides essential deformation information in cases when near-field observations are missing. For example, the 2002 Denali earthquake occurred during the data gap period, and thus, a near-field deformation map is still missing for most of the ruptured fault [e.g., *Lu et al.*, 2003; *Elliott et al.*, 2007]. With the method presented here, it should now be possible to extract details near the ruptured fault of this extraordinary event that were previously not captured. As large volumes of archived SAR images are now available from the many SAR missions, starting with Seasat in 1978, we may also be able to retrieve deformation signals for events that occurred during the 1980s; that is, by using images acquired by Seasat, spaceborne imaging

radar-C/X-band synthetic aperture radar instruments, and ERS. This would, however, likely require additional work due to the amplitude difference arising from the significantly different imaging geometries. A possible solution to calibrate the geometric effects in SAR amplitude images (e.g., due to shortening) is to use topographic data. Besides earthquake studies, the presented method is also applicable to various other geologic processes, such as landslides, volcanic eruptions, and dike intrusions.

Acknowledgments

The presented offsets and model parameters are available in the supporting information. Published source models used in Figures 4d and 4e are from the finite-source rupture model database (<http://equake-rc.info/SRCMOD/>). We thank Alex Copley (Cambridge University) for providing the InSAR and leveling data and Jean-Philippe Avouac (Cambridge University) for useful discussions. The ERS and Envisat SAR data were provided by the ESA through category-1 project 6703. The reported research was supported by King Abdullah University of Science and Technology (KAUST).

The Editor thanks Roland Bürgmann and an anonymous reviewer for their assistance in evaluating this paper.

References

- Antolik, M., and D. S. Dreger (2003), Rupture process of the 26 January 2001 M_w 7.6 Bhuj, India, earthquake from teleseismic broadband data, *Bull. Seismol. Soc. Am.*, *93*(3), 1235–1248.
- Ayoub, F., S. Leprince, and J. P. Avouac (2009), Co-registration and correlation of aerial photographs for ground deformation measurements, *ISPRS J. Photogramm. Remote Sens.*, *64*(6), 551–560.
- Bamler, R., and M. Eineder (2005), Accuracy of differential shift estimation by correlation and split-bandwidth interferometry for wideband and delta-k SAR systems, *IEEE Geosci. Remote Sens. Lett.*, *2*(2), 151–155.
- Bamler, R., and P. Hartl (1998), Synthetic aperture radar interferometry, *Inverse Probl.*, *14*(4), R1, doi:10.1088/0266-5611/14/4/001.
- Bechor, N. B., and H. A. Zebker (2006), Measuring two-dimensional movements using a single InSAR pair, *Geophys. Res. Lett.*, *33*, L16311, doi:10.1029/2006GL026883.
- Chandrasekhar, D., D. Mishra, B. Singh, V. Vijayakumar, and R. Bürgmann (2004), Source parameters of the Bhuj earthquake, India of January 26, 2001 from height and gravity changes, *Geophys. Res. Lett.*, *31*, L19608, doi:10.1029/2004GL020768.
- Chandrasekhar, D., R. Bürgmann, C. Reddy, P. Sunil, and D. Schmidt (2009), Weak mantle in NW India probed by geodetic measurements following the 2001 Bhuj earthquake, *Earth Planet. Sci. Lett.*, *280*(1–4), 229–235.
- Copley, A., J. Avouac, J. Hollingsworth, and S. Leprince (2011), The 2001 M_w 7.6 Bhuj earthquake, low fault friction, and the crustal support of plate driving forces in India, *J. Geophys. Res.*, *116*, B08405, doi:10.1029/2010JB008137.
- De Zan, F. (2014), Accuracy of Incoherent Speckle Tracking for Circular Gaussian Signals, *IEEE Geosci. Remote Sens. Lett.*, *11*(1), 264–267.
- Elliott, J. L., J. T. Freymueller, and B. Rabus (2007), Coseismic deformation of the 2002 Denali fault earthquake: Contributions from synthetic aperture radar range offsets, *J. Geophys. Res.*, *112*, B06421, doi:10.1029/2006JB004428.
- European Space Agency (2001), Project News: ERS, *ESA Earth Obs. Q.*, *69*, 4.
- Ferretti, A., C. Prati, and F. Rocca (2001), Permanent scatterers in SAR interferometry, *IEEE Trans. Geosci. Remote Sens.*, *39*(1), 8–20, doi:10.1109/36.898661.
- Gahalaut, V. K., and R. Bürgmann (2004), Constraints on the source parameters of the 26 January 2001 Bhuj, India, earthquake from satellite images, *Bull. Seismol. Soc. Am.*, *94*(6), 2407–2413.
- Hollingsworth, J., S. Leprince, F. Ayoub, and J. P. Avouac (2012), Deformation during the 1975–1984 Krafla rifting crisis, NE Iceland, measured from historical optical imagery, *J. Geophys. Res.*, *117*, B11407, doi:10.1029/2012JB009140.
- Hough, S. E., S. Martin, R. Bilham, and G. M. Atkinson (2002), The 26 January 2001 M 7.6 Bhuj, India, earthquake: Observed and predicted ground motions, *Bull. Seismol. Soc. Am.*, *92*(6), 2061–2079.
- Ji, C., D. J. Wald, and D. V. Helmberger (2002), Source description of the 1999 Hector Mine, California, earthquake. Part I: Wavelet domain inversion theory and resolution analysis, *Bull. Seismol. Soc. Am.*, *92*(4), 1192–1207.
- Jónsson, S., H. Zebker, P. Segall, and F. Amelung (2002), Fault slip distribution of the 1999 M_w 7.1 Hector Mine, California, earthquake, estimated from satellite radar and GPS measurements, *Bull. Seismol. Soc. Am.*, *92*(4), 1377–1389.
- Lee, J. S. (1986), Speckle suppression and analysis for synthetic aperture radar images, *Opt. Eng.*, *25*(5), 255636.
- Leprince, S., S. Barbot, F. Ayoub, and J.-P. Avouac (2007), Automatic and precise orthorectification, coregistration, and subpixel correlation of satellite images, application to ground deformation measurements, *IEEE Trans. Geosci. Remote Sens.*, *45*(6), 1529–1558.
- Lu, Z., T. Wright, and C. Wicks (2003), Deformation of the 2002 Denali fault earthquakes, mapped by Radarsat-1 interferometry, *Eos Trans. AGU*, *84*(41), 425–431, doi:10.1029/2003EO410002.
- Massonnet, D., M. Rossi, C. Carmona, F. Adragna, G. Peltzer, K. Feigl, and T. Rabaute (1993), The displacement field of the Landers earthquake mapped by radar interferometry, *Nature*, *364*(6433), 138–142.
- Michel, R., J.-P. Avouac, and J. Taboury (1999), Measuring ground displacements from SAR amplitude images: Application to the Landers earthquake, *Geophys. Res. Lett.*, *26*(7), 875–878, doi:10.1029/1999GL900138.
- Negishi, H., J. Mori, T. Sato, R. Singh, S. Kumar, and N. Hirata (2002), Size and orientation of the fault plane for the 2001 Gujarat, India earthquake (M_w 7.7) from aftershock observations: A high stress drop event, *Geophys. Res. Lett.*, *29*(20), 10–1–10–4, doi:10.1029/2002GL015280.
- Pathier, E., E. J. Fielding, T. J. Wright, R. Walker, B. E. Parsons, and S. Hensley (2006), Displacement field and slip distribution of the 2005 Kashmir earthquake from SAR imagery, *Geophys. Res. Lett.*, *33*, L20310, doi:10.1029/2006GL027193.
- Perissin, D., C. Prati, M. E. Engdahl, and Y. L. Desnos (2006), Validating the SAR wavenumber shift principle with the ERS-Envisat PS coherent combination, *IEEE Trans. Geosci. Remote Sens.*, *44*(9), 2343–2351.
- Rosen, P. A., S. Hensley, G. Peltzer, and M. Simons (2004), Updated repeat orbit interferometry package released, *Eos Trans. AGU*, *85*(5), 47–47, doi:10.1029/2004EO050004.
- Sansosti, E., P. Berardino, M. Manunta, F. Serafino, and G. Fornaro (2006), Geometrical SAR image registration, *IEEE Trans. Geosci. Remote Sens.*, *44*(10), 2861–2870.
- Santoro, M., J. Askne, U. Wegmuller, and C. Werner (2007), Observations, Modeling, and Applications of ERS-ENVISAT Coherence Over Land Surfaces, *IEEE Trans. Geosci. Remote Sens.*, *45*(8), 2600–2611.
- Schmidt, D. A., and R. Bürgmann (2006), InSAR constraints on the source parameters of the 2001 Bhuj earthquake, *Geophys. Res. Lett.*, *33*, L022315, doi:10.1029/2005GL025109.
- Singh, S. K., J. F. Pacheco, B. K. Bansal, X. Pérez-Campos, R. S. Dattatrayam, and G. Suresh (2004), A source study of the Bhuj, India, earthquake of 26 January 2001 (M_w 7.6), *Bull. Seismol. Soc. Am.*, *94*(4), 1195–1206.
- Wallace, K., R. Bilham, F. Blume, V. K. Gaur, and V. Gahalaut (2006), Geodetic constraints on the Bhuj 2001 earthquake and surface deformation in the Kachchh Rift Basin, *Geophys. Res. Lett.*, *33*, L10301, doi:10.1029/2006GL025775.
- Wang, T., and S. Jónsson (2015), Improved SAR amplitude image offset measurements for deriving three-dimensional coseismic displacements, *IEEE J. Sel. Top. Appl. Earth Obs. Remote Sens.*, *18*, doi:10.1109/JSTARS.2014.2387865.

- Wang, T., S. Jónsson, and R. F. Hanssen (2014), Improved SAR image coregistration using pixel-offset series, *IEEE Geosci. Remote Sens. Lett.*, *11*(9), 1465–1469.
- Wegmüller, U., M. Santoro, C. Werner, T. Strozzi, A. Wiesmann, and W. Lengert (2009), DEM generation using ERS–ENVISAT interferometry, *J. Appl. Geophys.*, *69*(1), 51–58.
- Zebker, H. A., and J. Villasenor (1992), Decorrelation in interferometric radar echoes, *Geosci. Remote Sens.*, doi:10.1109/36.175330.